Journal of Sound and Vibration (2000) **230**(3), 561–589
doi:10.1006/jsvi.1999.2630, available online at http://www.idealibrary.com on IDEAL®

TIME DOMAIN ESTIMATION OF RESPONSE AND INTENSITY IN BEAMS USING WAVE DECOMPOSITION AND RECONSTRUCTION

B. R. MACE AND C. R. HALKYARD†

Department of Mechanical Engineering, The University of Auckland, Private Bag 92019, *Auckland, New Zealand*

(*Received* 29 *June* 1998, *and in final form* 4 *August* 1999)

A method is described by which instantaneous values of the response, the internal forces and the intensity in beams can be estimated as functions of time. The individual components of intensity which propagate in each direction and the components due to shear and moment can also be estimated. The estimates are provided in real time by digitally filtering the outputs of an array of sensors. The digital filters are designed in the frequency domain using a wave decomposition approach and reconstructed in the time domain as FIR filters in this paper. The design and implementation process is described, numerical simulations of measurements in the farfield performed and an experimental implementation presented. The method is relatively insensitive to sensor miscalibration and measurement noise compared to other approaches, and yields instantaneous estimates as well as time averages.

1. INTRODUCTION

In this paper a technique for the time domain measurement of structural response and intensity is described. The technique is based on a wave decomposition and reconstruction approach. The outputs of an array of sensors are digitally filtered to provide estimates of any desired response quantity such as beam rotation, shear force, bending moment and so on, as well as net intensity and the components of the intensity which flow in each direction along the beam. The sensors may be of any form, such as accelerometers or non-contact devices.

While the approach described is applicable to the estimation of any response quantity, the emphasis in this paper is placed somewhat on the estimation of intensity, that is, the flow of vibrational energy through a structure, and its components. The measurement of intensity has attracted significant attention in the last few decades or so. However, practical applications are relatively few, especially

† This work was carried out while the author was at Industrial Research Ltd., P.O. Box 2225, Auckland, New Zealand.

0022-460X/00/080561 + 29 $35.00/0

compared to the measurement of acoustic intensity, which has become a valuable tool for the engineer.

To estimate intensity, vibration measurements are taken and can then be processed in a number of ways. One of the earliest and most common techniques involves applying finite difference approximations to estimate spatial derivatives of response from point measurements taken using an array of sensors [1, 2]. This gives intensity estimates in the time domain. For a beam this requires the measurement of acceleration (or, equivalently, velocity) at four equally and closely spaced points. In the far field, however, the time-average intensity can be estimated by time averaging the outputs of just two accelerometers. However, the method is sensitive to noise and to sensor miscalibration, and especially to any phase mismatch there may be between the sensors.

Other techniques, such as the cross-spectrum [3] and wave decomposition methods [4], rely on batch processing and are frequency domain techniques. The responses are measured over a period of time and later Fourier-analyzed to give estimates of the total intensity over the measurement period and over a range of frequencies.

In this paper, a technique for the time domain estimation of intensity is described. An array of sensors is used to measure the vibrational response and the sensor outputs are then filtered in the time domain to provide the estimates of response, internal forces and intensity. This filtering would normally be done digitally. The coefficients of the filters are designed using a wave decomposition approach in the frequency domain. The method can be implemented in real time to give estimates of instantaneous net intensity and the components of intensity in different directions. It is applicable to transient or random excitation, be it stationary or not. The estimates can be time-averaged if required, or subsequently Fourier-analyzed to give frequency domain estimates. The wave decomposition approach used here is somewhat similar to that used in some active control studies [5, 6].

Here the method is developed with particular reference to bending vibrations in beams. The approach is systematic, in that a design procedure is described which allows for the use of any type of sensor, such as accelerometers and strain gauges, and can be applied to the measurement of intensity in any wave-bearing structural component. Hybrid sensor arrays, which utilize two or more types of sensor and which have distinct advantages [4], may be used and the sensors need not be equally spaced. Furthermore, the estimates are relatively insensitive to measurement noise and sensor miscalibration.

In the next section some results concerning intensity and wave motion in beams are reviewed. This is followed by descriptions of the frequency domain design procedure and its implementation in the time domain. Results of numerical simulations are presented and an experimental implementation is described. These examples concern farfield estimation using two accelerometers. The performance of various sensor systems is considered elsewhere, as is the application to intensity measurement in plates.

2. ENERGY FLOW AND WAVES IN BEAMS

Consider a thin beam lying along the x-axis as shown in Figure 1. If the effects of shear deformation and rotary inertia can be neglected then the displacement

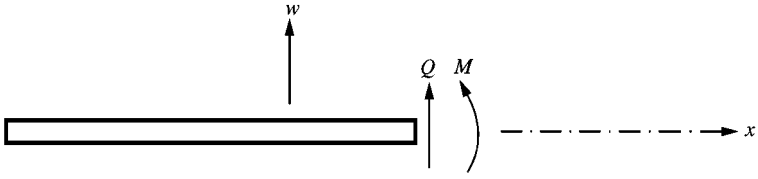

Figure 1. Definition of positive shear force and bending moment.

$w(x, t)$ satisfies

$$EI\frac{\partial^4 w}{\partial x^4} + \rho\frac{\partial^2 w}{\partial t^2} = p(x, t), \tag{1}$$

where EI and ρ are the bending stiffness and mass per unit length of the beam and $p(x, t)$ is the applied force per unit length. A list of symbols is given in Appendix A. The corresponding shear force $q(x, t)$ and bending moment $m(x, t)$ as defined in Figure 1 are

$$m = EI\frac{\partial^2 w}{\partial x^2}, \quad q = -EI\frac{\partial^3 w}{\partial x^3}, \tag{2}$$

The flow of energy along the beam, i.e., the structural intensity, is given in terms of the beam deformation and internal forces by

$$i(x, t) = -qv - m\dot{\theta}, \quad v = \frac{\partial w}{\partial t}, \quad \dot{\theta} = \frac{\partial^2 w}{\partial x\,\partial t}, \tag{3}$$

where v and $\dot{\theta}$ are the transverse and rotational velocities of the beam. The intensity can be estimated quite straightforwardly if these velocities and internal forces are known. In practice, however, it is difficult (or perhaps impossible) to measure the internal forces. Normally, the beam response is instead measured at a number of points and the internal forces then inferred from equation (2). One example is that of the finite difference approach [1], which in general requires four sensors, so that the shear force (which involves the third spatial derivative) can be estimated. This paper describes methods of estimating these internal forces and the rotational velocity using a wave decomposition approach. From these estimates other quantities, such as the intensity, may then be found.

In many applications, primarily those involving stationary, random excitation or if the excitation is deterministic and repeatable (especially within the laboratory), the time-average intensity $\langle i(t)\rangle$ may be of most interest. This may, of course, be found by time-averaging the instantaneous intensity. This time average is also equal to an estimate that can be provided by a finite difference approach [1], in which the acceleration and velocity are measured at two closely spaced points, namely

$$\langle i\rangle = \frac{\sqrt{EI\rho}}{\pi\Delta f_c}\langle \ddot{w}_1\, \ddot{w}_2\rangle, \tag{4}$$

where Δ is the sensor spacing and f_c the centre of the frequency band under consideration. (Throughout this paper a measured variable such as velocity is assumed to be equivalent to its time derivative, acceleration. In practice, one can be found from the other by analogue integration or differentiation.)

2.1. WAVES AND ENERGY FLOW

Suppose now that all quantities vary time harmonically as $\exp(\mathrm{i}\omega t)$. The beam displacement can be written as

$$w(x,t) = \mathrm{Re}\{W(x,\omega)e^{\mathrm{i}\omega t}\}. \tag{5}$$

In this paper, the notation is adopted in which the lower- and upper-case symbols, e.g., $w(t)$ and $W(\omega)$, represent the same variable in the time and frequency domains respectively and the explicit time dependence $\exp(\mathrm{i}\omega t)$ will normally be suppressed. In a region in which no applied forces act, the displacement can be expressed as the sum of wave components:

$$W(\omega) = \Phi_W^+(\omega)\mathrm{e}^{-\mathrm{i}kx} + \Phi_{N,W}^+(\omega)\mathrm{e}^{-kx} + \Phi_W^-(\omega)\mathrm{e}^{\mathrm{i}kx} + \Phi_{N,W}^-(\omega)\mathrm{e}^{kx}, \tag{6}$$

where $\Phi_W^{\pm}$ are the complex amplitudes of the positive- and negative-going propagating waves and $\Phi_{N,W}^{\pm}$ those of the positive- and negative-going nearfields. The nearfield components decay exponentially in the positive and negative x directions respectively. In equation (6) $k = \sqrt[4]{\rho\omega^2/EI}$ is the wavenumber. In the presence of damping, k has a (usually small) negative imaginary part so that the amplitude of a propagating wave component decays gradually in the direction of propagation. In this paper, it will be assumed that this decay is negligible over distances of the order of the sensor separations.

The subscript W in equation (6) indicates that it is the displacement $W(\omega)$ of the beam that has been decomposed into the wave components Φ_W. The wave amplitudes Φ_W are thus referred to as displacement wave amplitudes. However, all response quantities (velocity, acceleration, shear force, etc.) vary time harmonically under the passage of a wave. Thus, one could equally define the amplitudes of the wave components in terms of the amplitude of any such response quantity. For example, one may equally refer to velocity waves, which have amplitudes $\Phi_V = \mathrm{i}\omega\Phi_W$, or acceleration waves which have amplitudes $\Phi_A = -\omega^2\Phi_W$: the superposition of these waves then gives the velocity or acceleration of the waveguide respectively. Whichever is chosen is purely a matter of convenience.

2.1.1. *Intensity and wave components*

The shear force at $x = 0$ can be written in terms of wave components as

$$q(t) = \mathrm{Re}\{Q(\omega)\mathrm{e}^{\mathrm{i}\omega t}\},\ Q(\omega) = EIk^3(-\mathrm{i}\Phi_W^+(\omega) + \Phi_{N,W}^+(\omega) + \mathrm{i}\Phi_W^-(\omega) - \Phi_{N,W}^-(\omega)), \tag{7}$$

and hence the shear contribution to the intensity is

$$-q(t)v(t) = -\operatorname{Re}\{Q(\omega)e^{i\omega t}\}\operatorname{Re}\{i\omega W(\omega)e^{i\omega t}\}. \tag{8}$$

There is also a moment component to the total intensity.

By decomposing the response variables into wave components, it is clear that the total intensity has contributions involving the interactions of all these components. The terms involving $\Phi^+\Phi^+$ describe the energy flow associated with the positive-going wave alone: these terms give shear and moment contributions to the total intensity which are equal in magnitude, vary at a frequency 2ω and are out of phase, so that their sum is constant, independent of time. Similarly, the intensity arising from the terms involving $\Phi^-\Phi^-$ is constant. The interactions between the positive- and negative-propagating waves (i.e., the $\Phi^+\Phi^-$ terms), however, give no contribution to the total intensity since their shear and moment contributions are equal and opposite, so that they always sum to zero. The nearfields individually (i.e., the $\Phi_N^+\Phi_N^+$ and $\Phi_N^-\Phi_N^-$ terms) also have shear and moment components which are equal and opposite, giving a zero contribution to the total intensity, as do the interactions of a propagating component with a nearfield. The nearfield interaction terms, however (i.e., the $\Phi_N^+\Phi_N^-$ terms) give a contribution which depends on the relative phases of the wave components. This term can be substantial if both nearfields have significant amplitudes.

Thus, the total intensity in the beam arises from three terms: the two propagating waves independently and the interaction of the two nearfields.

2.1.2. *Directional components of intensity and propagating waves—"power waves"*

In the absence of substantial nearfields, the intensity can be divided into positive- and negative-flowing components, each of which comprises shear and moment contributions. If the wave amplitudes $\Phi^\pm$ are known, then these can be found straightforwardly. However, it is convenient, perhaps, to define "power waves" $\Phi_P^+(\omega)$ and $\Phi_P^-(\omega)$ (in a manner analogous to displacement and velocity waves) as waves whose amplitudes are such that $\frac{1}{2}|\Phi_P^+(\omega)|^2$ and $\frac{1}{2}|\Phi_P^-(\omega)|^2$ give the power in the positive and negative x directions respectively. There are both shear and moment power waves, their amplitudes being defined in terms of displacement and velocity wave amplitudes by

$$\begin{aligned} \Phi_{P,q}^\pm &= i\sqrt{EIk^3\omega}\ \Phi_W^\pm = \sqrt[4]{EI\rho}\,\sqrt{k}\,\Phi_V^\pm, \\ \Phi_{P,m}^\pm &= \sqrt{EIk^3\omega}\ \Phi_W^\pm = -i\sqrt[4]{EI\rho}\,\sqrt{k}\,\Phi_V^\pm, \end{aligned} \tag{9}$$

2.1.3. *Reconstruction in the time domain*

In general, more than one frequency component will be present and any response variable is given by superposition. For example, the positive going displacement wave amplitude can be written as

$$\phi_w^+(t) = F^{-1}\{\Phi_W^+(\omega)\} = \int_{-\infty}^{\infty} \Phi_W^+(\omega)e^{i\omega t}\,d\omega, \tag{10}$$

where $F^{-1}(\cdot)$ is the inverse Fourier transform. Any response quantity, be it beam displacement, shear force, positive-going wave amplitude or whatever, can be found in a similar manner.

3. WAVE DECOMPOSITION, RECONSTRUCTION AND INTENSITY ESTIMATION

3.1. INTRODUCTION

An array of n sensors is mounted on the beam as shown in Figure 2. It is assumed that no external excitations act in this region. The aim is to use the sensor outputs $s_j(t), j = 1, 2, \ldots, n$, to estimate various response quantities at some location on the beam. These response quantities may include $w(t)$, $q(t)$, etc., or the intensity $i(t)$. The sensors may give point measurements of acceleration or velocity, for example, or may instead be distributed (e.g., strain gauges of non-negligible length). The array may contain sensors of different kinds, such an array being referred to as a hybrid sensor array.

The means by which this response estimation may be performed is described in this section. The sensor outputs are first used to estimate the wave amplitudes in the measurement region. By reconstruction, any response quantity can be expressed as a sum of contributions from these wave amplitudes. Time domain estimates are made by digital filtering, i.e., by the convolution of the sensor outputs with the coefficients of various digital filters. The implemented filters have frequency responses which approximate idealized designs, the design being performed in the frequency domain. In this section, this design approach is described and time domain implementation discussed with reference to some example sensor systems.

3.2. WAVE DECOMPOSITION IN THE FREQUENCY DOMAIN

Assume that all quantities vary time-harmonically. Let the displacement wave amplitudes at $x = 0$ be given by

$$\mathbf{\Phi}_W(\omega) = [\Phi_W^+ \;\; \Phi_W^- \;\; \Phi_{N,W}^+ \;\; \Phi_{N,W}^-]^{\mathrm{T}}, \tag{11}$$

where it is assumed that both propagating and nearfield components are present. In many applications one or more components will have negligible amplitude—for

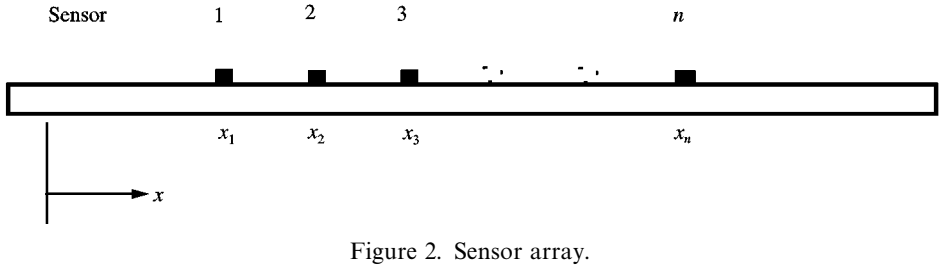

Figure 2. Sensor array.

example, in the farfield both nearfield terms can be neglected. In such situations, the appropriate component(s) can then be ignored.

The sensor outputs $S_j(\omega)$ are related to $\mathbf{\Phi}$ by

$$\mathbf{S}(\omega) = \mathbf{F}(\omega)\mathbf{\Phi}(\omega), \tag{12}$$

where

$$\mathbf{S}(\omega) = [S_1 \;\; S_2 \cdots S_n]^{\mathrm{T}}. \tag{13}$$

In equation (12), $\mathbf{F}$ is a matrix, the jth row of which depends on the type of the jth sensor and its location with respect to the origin. For example, for an accelerometer located at x_j

$$S_j(\omega) = -\omega^2 [\exp(-\mathrm{i}kx_j)\exp(\mathrm{i}kx_j)\exp(-kx_j)]\mathbf{\Phi}_W(\omega), \tag{14}$$

while for a strain gauge of length d centered at x_j,

$$S_j(\omega) = -zk^2 \left[\frac{\sin kd}{kd} \mathrm{e}^{-\mathrm{i}kx_j} \quad \frac{\sin kd}{kd} \mathrm{e}^{\mathrm{i}kx_j} \quad \frac{\sinh kd}{kd} \mathrm{e}^{-kx_j} \quad \frac{\sinh kd}{kd} \mathrm{e}^{-kx_j} \right] \mathbf{\Phi}_W(\omega), \tag{15}$$

where z is the distance from the strain gauge to the neutral axis. The wave amplitudes are therefore given by

$$\mathbf{\Phi}_W(\omega) = \mathbf{F}^{-1}(\omega)\mathbf{S}(\omega), \tag{16}$$

where the inverse is assumed to exist. Normally, for a given sensor array configuration, $\mathbf{F}$ will be singular at certain frequencies which depend on the sensor spacing, and hence the lowest such frequency limits the frequency range in which such a configuration is usable. For the case of an overdetermined measurement array, in which there are more sensors than wave components, the inverse is assumed to be evaluated in the least-squares sense, i.e.,

$$\mathbf{F}^{-1} = [\mathbf{F}^{\mathrm{H}}\mathbf{F}]^{-1}\mathbf{F}^{\mathrm{H}}, \tag{17}$$

where the superscript H denotes the complex conjugate transpose (the Hermitian). Overdetermined arrays can prove much less sensitive to noise, miscalibration and other measurement errors.

Any response quantity $P(\omega)$ can be related to the wave amplitudes by an expression of the form

$$P(\omega) = \mathbf{H}_{P,\Phi}(\omega)\mathbf{\Phi}_W(\omega), \tag{18}$$

where $\mathbf{H}_{P,\Phi}$ is a row vector which relates the wave amplitudes to the response variable $P(\omega)$. For example, for the displacement, slope, bending moment and shear

force at $x = 0$ the appropriate vectors are given by

$$\begin{aligned}
\mathbf{H}_{W,\Phi}(\omega) &= [1 \;\; 1 \;\; 1 \;\; 1] \\
\mathbf{H}_{\Theta,\Phi}(\omega) &= k[-i \;\; i \;\; -1 \;\; 1\} \\
\mathbf{H}_{M,\Phi}(\omega) &= -EIk^2[1 \;\; 1 \;\; -1 \;\; -1] \\
\mathbf{H}_{Q,\Phi}(\omega) &= -EIk^3[i \;\; -i \;\; -1 \;\; 1].
\end{aligned} \tag{19}$$

Time derivatives follow from multiplication by the corresponding power of $(\mathrm{i}\omega)$ (e.g., $\mathbf{H}_{V,\Phi} = \mathrm{i}\omega\mathbf{H}_{W,\Phi}$). Consequently, the frequency responses relating sensor measurements to the response variable P are

$$P(\omega) = \mathbf{H}_P(\omega)\mathbf{S}(\omega) = \sum_{j=1,n} H_{P,j}(\omega)S_j(\omega), \quad \mathbf{H}_P = \mathbf{H}_{P,\Phi}\mathbf{F}^{-1}, \tag{20}$$

where $\mathbf{H}_P$ is a row vector of frequency responses which relate the sensor outputs to the response variable $P(\omega)$. Thus, any response quantity can be found by appropriately filtering the sensor outputs, i.e., by multiplying the sensor outputs by appropriate frequency responses and summing.

3.3. RECONSTRUCTION: TIME DOMAIN RESPONSE ESTIMATION

In general, the time response will be a superposition of many frequency components and is given by an inverse Fourier transform as in equation (10). Any response quantity $p(t)$ can thus be found by evaluating the inverse transform of equation (20). Since the inverse transform of a product is equal to the convolution of the individual inverse transforms, then

$$p(t) = \mathbf{h}_p(t) * \mathbf{s}(t) = \sum_{j=1,n} h_{p,j}(t) * s_j(t), \tag{21}$$

where $*$ denotes convolution and where $h_{p,j}(t)$ is the inverse Fourier transform of $H_{P,j}(\omega)$, that is, the impulse response of a filter whose frequency response is $H_{P,j}(\omega)$. Also, $\mathbf{h}_p(t)$ is the corresponding row vector of impulse responses.

One issue that arises is that the required filters, i.e., those with impulse responses $h_{p,j}(t)$, are typically non-causal, so that $h_{p,j}(t)$ is non-zero for $t < 0$. Such non-causality means that the response $p(t)$ at some time is determined not only by past and present sensor measurements, but also by future ones. This behaviour is not surprising, since estimates are made from sensor measurements taken at various locations. It takes some time for waves to propagate from one location to another, so exact estimation of wave amplitudes, for example, requires knowledge of the future output of the downstream sensor. In practice, these effects are unimportant for response and intensity estimation when "real-time" performance is not crucial—in effect a small delay can be incorporated into the filtering process

before a response estimate is produced. These time delays have more profound consequences for applications such as active control.

Practical implementations will be predominantly digital. The sensor outputs are sampled at the sampling frequency f_s, being first passed through anti-aliasing, low-pass filters with a cut-off frequency of somewhat less than the Nyquist frequency $f_n = f_s/2$. This, therefore, defines a maximum frequency of interest and often, as in the example in section 3.4 below, a maximum transducer spacing. The sensor outputs are sampled, yielding $s_{j,m}$ at time step m. The desired frequency responses H_P are defined at discrete, equally spaced frequencies. The variable p_m at time step m is then given by digitally filtering $s_{j,m}$ with a digital filter whose frequency response approximates the ideal, H_P. There are two main forms for such digital filters, namely finite impulse response (FIR) and infinite impulse response (IIR) filters, and there exist a number of ways in which the coefficients of such filters can be found [7]. In an FIR filter implementation, equation (21) becomes

$$p_m = \sum_{j=1,n} \left\{ \sum_{k=0,K} h_{p,j,k}\, s_{j,m-k} \right\}, \tag{22}$$

where the response p_m at time step m depends on present and previous values of the sensor measurements s_j and on the $K+1$ filter coefficients $h_{p,j,k}$ for each of the n sensors. Only FIR filters are used in the numerical and experimental studies below. In an IIR filter, p depends also on previous values of p. Such filters normally give a better approximation to the desired frequency response for a given filter order but can be unstable.

The problem of causality can be overcome by allowing a finite delay of r time steps, which is equivalent to multiplying H by $\exp(-\mathrm{i}\omega r/f_s)$. A causal filter will then produce an estimate of the value of p_m at time step $m+r$. In the examples below only small values of r are required so that the time delays involved are unimportant, especially if time averages are desired.

One method of designing an FIR approximation to the frequency responses in equation (20) is as follows. The time delay of r steps is introduced and a $(2r+1)$ coefficient FIR filter designed to approximate $H(\omega)\exp(-\mathrm{i}r\omega/f_s)$. The coefficients h_k, $k = 0 \ldots 2r$, are then evaluated so that the implemented frequency response $\hat{H} = \sum_{k=0,2r} h_k \exp(-\mathrm{i}\omega k/f_s)$ is the best approximation to H in the least-squares sense, i.e., so as to minimize the sum over frequency of $(|H(\omega) - \hat{H}(\omega)|^2)$. If it is felt necessary, a weight $\sigma(\omega)$ can be introduced and $(\sigma(\omega)|H(\omega) - \hat{H}(\omega)|^2)$ minimized.

3.3.1. *Intensity estimation*

The instantaneous, net intensity can be estimated from equation (3) once estimates of the instantaneous velocity, shear force, angular velocity and bending moment at a point have been made. This also directly yields estimates of the components due to shear and bending independently.

Estimates can also be made of the instantaneous components of intensity in both the positive and negative x directions. These can be found by estimating the contributions to the velocity, shear force, etc., from each wave component

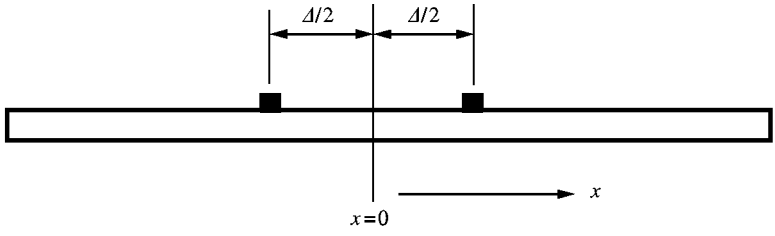

Figure 3. Two accelerometer array.

(e.g., $\Phi_W^{\pm}$), hence finding the corresponding component of the intensity. Alternatively, the power wave amplitudes $\Phi_{P,q}^{\pm}$ and $\Phi_{P,m}^{\pm}$ themselves can be estimated and the power associated with each found as described in section 2.1.2.

Time averaging can also be performed straightforwardly, for example by passing the instantaneous estimate of intensity through a moving-average (MA) filter. This inevitably introduces additional delays, which are typically very much larger than those arising from non-causality.

3.4. EXAMPLE: TWO ACCELEROMETERS IN THE FAR FIELD

In the far field there are only two wave components, the nearfields being negligible, and hence two sensors are sufficient to determine the response. Figure 3 shows a system comprising two accelerometers a distance Δ apart, such a system being perhaps the simplest and most common system for structural intensity estimation. The aim is to estimate the response (e.g., velocity, shear force, net intensity) at $x = 0$.

The sensor measurements $S_{1,2}$ are here taken to be the measured velocities[†] $v_{1,2}(t)$ at positions $x_{1,2} = \pm \Delta/2$ and hence $S_{1,2}(\omega) = V_{1,2}(\omega) = \mathrm{i}\omega W_{1,2}(\omega)$. The matrix $\mathbf{F}$ is given by

$$\mathbf{F} = \mathrm{i}\omega \begin{bmatrix} \exp(\mathrm{i}k\Delta/2) & \exp(-\mathrm{i}k\Delta/2) \\ \exp(-\mathrm{i}k\Delta/2) & \exp(\mathrm{i}k\Delta/2) \end{bmatrix} \tag{23}$$

while its inverse, which relates displacement wave amplitudes to the measured velocities becomes

$$\mathbf{F}^{-1} = -\frac{1}{2\omega \sin k\Delta} \begin{bmatrix} \exp(\mathrm{i}k\Delta/2) & -\exp(-\mathrm{i}k\Delta/2) \\ -\exp(-\mathrm{i}k\Delta/2) & \exp(\mathrm{i}k\Delta/2) \end{bmatrix}. \tag{24}$$

Using the first two columns of equation (19) (since nearfields are neglected) and equation (24) the frequency responses relating the velocities and internal forces at

[†]These may be found, for example, by analogue integration of measured accelerations. Velocities are taken here for convenience in presenting numerical results.

the array centre to the measured velocities are found to be

$$\mathbf{H}_V(\omega) = \frac{1}{2\cos(k\Delta/2)}[1 \;\; 1],$$

$$\mathbf{H}_\Theta(\omega) = \frac{(k\Delta/2)}{\Delta\sin(k\Delta/2)}[-1 \;\; 1]$$

$$\mathbf{H}_M(\omega) = \frac{i\sqrt{EI\rho}}{2\cos(k\Delta/2)}[1 \;\; 1]$$

$$\mathbf{H}_Q(\omega) = \frac{i\sqrt{EI\rho}\,(k\Delta/2)}{\Delta\sin(k\Delta/2)}[1 \;\; -1] \tag{25}$$

and thus involve the sums and differences of the two measured velocities. Note that some of the frequency responses become infinite when $k\Delta = \pi$, so that there is some maximum allowable separation for measurement within a given frequency range—the sensors must be less than half the shortest wavelength apart.

The frequency responses relating the velocity wave amplitudes to the measured velocities are given by

$$\mathbf{H}_{\Phi_V^+} = \mathbf{H}_{\Phi_V,1} - \mathbf{H}_{\Phi_V,2},$$

$$\mathbf{H}_{\Phi_V^-} = \mathbf{H}_{\Phi_V,1} + \mathbf{H}_{\Phi_V,2},$$

$$\mathbf{H}_{\Phi_V,1} = \frac{1}{4\cos(k\Delta/2)}[1 \;\; 1], \;\; \mathbf{H}_{\Phi_V,2} = \frac{\mathrm{i}}{4\sin(k\Delta/2)}[1 \;\; -1], \tag{26}$$

while the power wave amplitudes are found from

$$\mathbf{H}_{\Phi_{P,q}^+} = \mathbf{H}_{\Phi_{P,q},1} - \mathbf{H}_{\Phi_{P,q},2}, \qquad \mathbf{H}_{\Phi_{P,q}^-} = \mathbf{H}_{\Phi_{P,q},1} + \mathbf{H}_{\Phi_{P,q},2},$$

$$\mathbf{H}_{\Phi_{P,m}^+} = \mathbf{H}_{\Phi_{P,m},1} - \mathbf{H}_{\Phi_{P,m},2}, \qquad \mathbf{H}_{\Phi_{P,m}^-} = \mathbf{H}_{\Phi_{P,m},1} + \mathbf{H}_{\Phi_{P,m},2},$$

$$\mathbf{H}_{\Phi_{P,q},1} = \left(\frac{\sqrt[4]{EI\rho}}{2\sqrt{\Delta}}\right)\frac{\sqrt{k\Delta/2}}{\cos(k\Delta/2)}[1 \;\; 1] \qquad \mathbf{H}_{\Phi_{P,q},2} = \left(\frac{\sqrt[4]{EI\rho}}{2\sqrt{\Delta}}\right)\frac{\mathrm{i}\sqrt{k\Delta/2}}{\sin(k\Delta/2)}[1 \;\; -1]$$

$$\mathbf{H}_{\Phi_{P,m},1} = -\,\mathrm{i}\mathbf{H}_{\Phi_{P,q},1}, \qquad \mathbf{H}_{\Phi_{P,m},2} = -\,\mathrm{i}\mathbf{H}_{\Phi_{P,q},2}. \tag{27}$$

Block diagram representations of these two approaches to intensity estimation are shown in Figure 4.

FIR approximations to the ideal frequency responses of equations (25–27) can be found using the least-squares technique outlined above. Some examples are shown

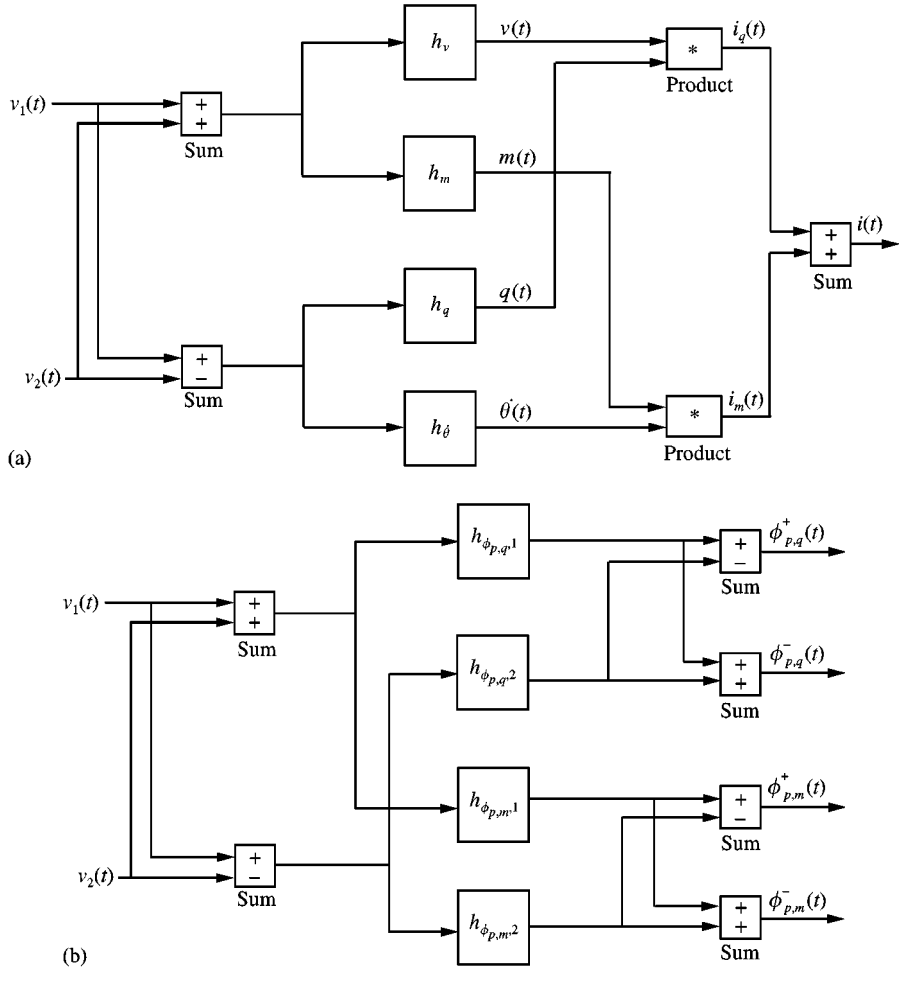

Figure 4. Block diagram representations: (a) estimation of internal forces, velocities and intensity and (b) estimation of power wave amplitudes.

in Figure 5, in which various ideal frequency responses H and their implemented approximations $\hat{H}$ are shown for various filter lengths. Figure 6 shows the actual filter coefficients. The frequency responses were defined at 512 equally spaced frequencies up to the Nyquist frequency and the filter coefficients found using uniform weighting over the whole frequency range.

The real frequency responses H_V, $H_{\dot{\Theta}}$, $H_{\Phi_{P,q},1}$ and $H_{\Phi_{P,m},2}$ are approximated very well with very few terms. For these the FIR filters are symmetric, in that $h_{r-j} = h_{r+j}$, and the higher order filter coefficients decrease asymptotically as $|r \pm j|^{-2}$.

Significantly more terms are required to approximate the pure imaginary frequency responses H_M, H_Q, $H_{\Phi_{P,q},2}$ and $H_{\Phi_{P,m},1}$. This is due in part to the fact that h_k are constrained to be real, and hence $\hat{H}$ must be zero at zero frequency and at the Nyquist frequency, introducing discontinuities in the frequency responses at those

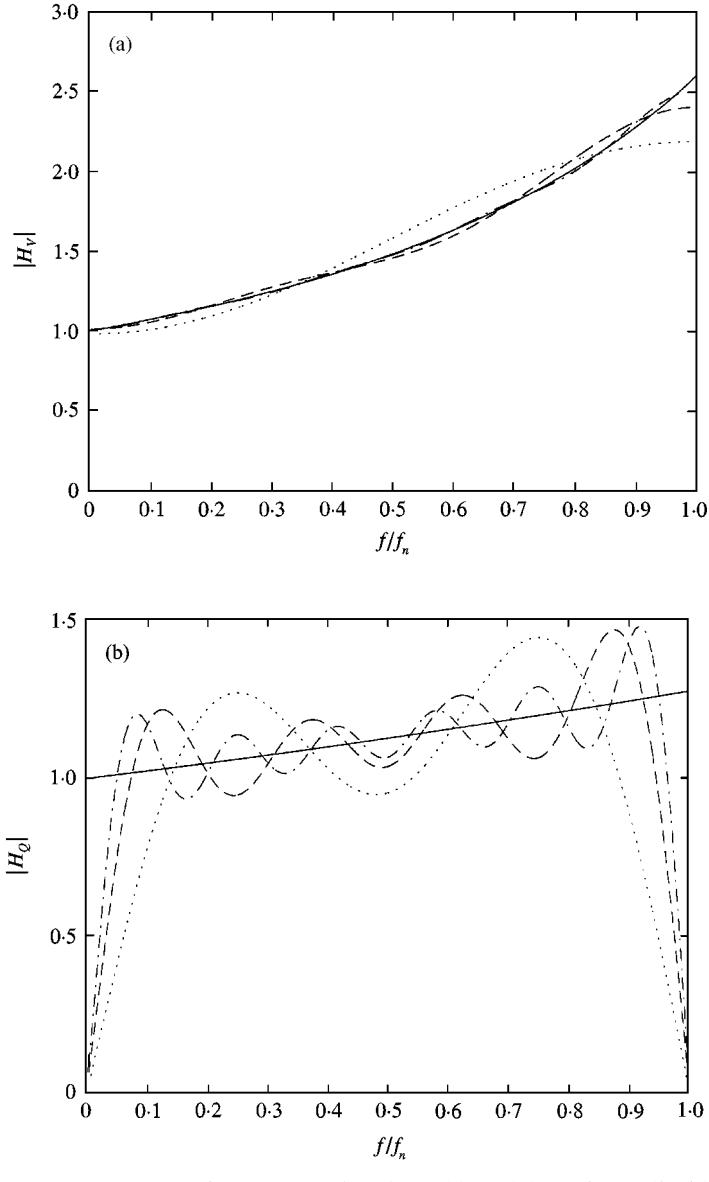

Figure 5. Frequency responses of FIR approximations: (a) $H_V(\omega) = 1/(2\cos(k\Delta/2))$; —, ideal; . . ., $r = 1$; - - -, $r = 3$; - . - ., $r = 7$. (b) $H_\varrho(\omega) = \mathrm{i}\sqrt{EI\rho}\,(k\Delta/2)/(\Delta \sin(k\Delta/2))$; —, ideal; . . ., $r = 3$; - - -, $r = 7$; - . - ., $r = 11$.

frequencies. These filters are also antisymmetric, so that $h_{r-j} = -h_{r+j}$. Furthermore, the higher order filter coefficients decrease asymptotically only as $|r \pm j|^{-1}$. Finally, in these cases the total filter length must be large enough to capture information about the low-frequency components, and hence the approximation is poor for frequencies below $f_N/(2r + 1)$ and for frequencies above $2rf_N/(2r + 1)$. However, it should be noted that in practice the low- and high-frequency components of the signals will often be filtered out (for example by

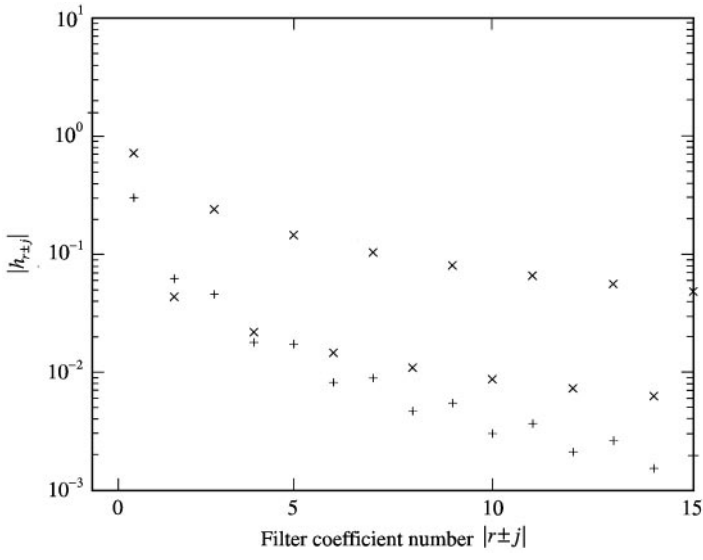

Figure 6. FIR filter coefficients, $r = 15$: $+ h_{v,}$; $\times h_q$.

the anti-aliasing filters and by AC coupling) and that this will substantially ameliorate the effects of the poor approximation in these frequency ranges. This is demonstrated in the numerical simulations of section 4 and the practical implementation of section 5.

It is worth emphasizing that the *phases* of the implemented filters $\hat{H}$ are *exact*, since the coefficients are either symmetric or antisymmetric about the filter centre. This is particularly relevant to the estimation of net intensity, especially in a wave field which is fairly reverberant, where estimation is known to be very sensitive to any phase mismatching.

3.5. EFFECTS OF NOISE AND MISCALIBRATION

In this section, some general comments are made regarding the effects of measurement noise and miscalibration. The actual effects in a particular implementation depend on the sensor configuration, the frequency content of the vibrations and so on. Particular reference is made to the two-transducer system discussed above and the finite difference estimate provided by the same system. In the latter case, the spacing of the sensors must be restricted to be much less than the wavelength to avoid a large bias error. Numerical examples are presented in section 4 below.

If the sensor measurements are contaminated with independent random noise of zero mean (e.g., $\hat{v}_{1,2}(t) = v_{1,2}(t) + \varepsilon_{1,2}(t)$ with $E[\varepsilon_{1,2}] = 0$), then the estimates of the wave amplitudes, internal forces, etc., will also be contaminated. In both the wave decomposition and finite difference approaches the error in the estimated intensity is of zero mean and its expected mean square value is of the order of $E[\varepsilon_1^2] + E[\varepsilon_2^2]$.

Numerical results indicate that the finite difference approach is somewhat more sensitive to noise.

Suppose that there exists some magnitude miscalibration between the sensors, so that the output of sensor 2, for example, is $\hat{v}_2(t) = (1 + \mu)v_2(t)$, where μ is some (small) constant. The estimate of intensity is then biased by the same amount μ, and this depends little on which approach is adopted.

The wave decomposition approach, however, is in general very much less sensitive to phase miscalibration (i.e., if $\hat{v}_2(t) = \exp(i\mu)v_2(t)$, with μ some (small) constant). The reason behind this is that estimation of intensity involves the difference between the two sensor outputs. In the finite difference methods, the sensors are constrained to be close to avoid errors from the finite difference approximation. Even small relative phase errors then produce large relative errors in this difference. In the wave decomposition approach, on the other hand, the sensor separation can be very much larger and the term $\exp(-ik\Delta)$ is introduced into equation (24), from which the wave amplitudes are estimated. A phase difference of the order of $k\Delta$ thus exists between the sensor outputs and the relative effect of phase miscalibration becomes correspondingly less.

3.6. SENSOR SYSTEMS

A further advantage of the wave decomposition approach is that it systematically allows for sensor systems of any form. For example, the separation need not be uniform, the system may be overdetermined and the sensors may be of different types (e.g., a mixture of accelerometers and strain gauges). Such hybrid systems have been shown to have significantly better performance than arrays of the same type of transducer [4] in many applications. The performances of various sensor systems are compared elsewhere.

4. NUMERICAL SIMULATIONS: FARFIELD ESTIMATION USING TWO POINT MEASUREMENTS

In this section the results of some numerical simulations are described. The intentions are to investigate the accuracy of the wave decomposition estimates, including estimates made in the presence of noise and miscalibration, and to compare the accuracy with that of the finite difference method.

The first stage is to simulate the response of a beam to excitation. This is done using a spectral approach [8] and yields time series giving any desired response quantity. These time series are typically very long. Briefly, suppose that a point force $f(t)$, defined at discrete times $n\tau$, acts at x_f. Its spectrum $F(\omega)$ is found by taking the FFT. The component at frequency ω introduces propagating and nearfield acceleration waves of amplitudes

$$\Phi_A^{\pm} = \frac{ikF}{4\rho}, \quad \Phi_{N,A}^{\pm} = \frac{kF}{4\rho} \tag{28}$$

at $x = x_f$. (It is convenient numerically to work in terms of acceleration wave amplitudes because of problems associated with the model as $\omega \to 0$, where force components produce displacements and velocities that tend to infinity.) These waves give a contribution to the acceleration spectrum at a location $x_r \geqslant x_f$ given by

$$A(\omega) = \Phi_A^+ \exp(-\mathrm{i}k(x_r - x_f)) + \Phi_{N,A}^+ \exp(-k(x_r - x_f)) \tag{29}$$

with a similar expression in terms of Φ_A^- and $\Phi_{N,A}^-$ if $x_r \leqslant x_f$. The total response spectrum is found by summing wave contributions from all applied forces and the response $a(t)$ then found by evaluating the inverse FFT. Other response quantities can be found in a similar way because their relationships to the wave amplitudes are known. These may be quantities such as shear force and velocity at some location, and hence the actual intensity at that location can be calculated by multiplication. Similarly, time series giving transducer outputs can be found (e.g., velocities at the sensor locations) and these used as inputs to the time domain intensity estimator.

Next, FIR filters are designed to approximate the ideal filters, these depending, of course, on the particular sensor array being considered, the type and number of sensors and the physical locations. The ideal frequency response is defined at a number of frequencies, the "non-causal" delay r chosen and a $2r + 1$ term FIR filter found using the least-squares method or otherwise.

The final stage is to implement the estimator in "real time" by passing the simulated time series through the FIR filter. Noise and miscalibration can be added to the sensor outputs if required.

In all the simulations described below the time series were $2^{15} = 32\,768$ points in length. Beam parameters are normalized by taking $EI = \rho = 1$, positions x on the beam are normalized with respect to the wavelength λ_n at the Nyquist frequency and estimates are made of response quantities at $x = 0$. Other response quantities are also found: these are the velocities at $x = \pm 0{\cdot}15\lambda_n$, which are used as inputs to the wave decomposition filters, the acceleration at $x = -0{\cdot}02\lambda_n$ and the velocity at $x = 0{\cdot}02\lambda_n$, the last two being used to provide estimates of the intensity using the difference approximation of equation (4). FIR filters are designed by a least-squares fit to the ideal frequency responses at 512 uniformly spaced frequencies up to the Nyquist frequency with uniform weighting. A time delay of $r = 7$ is used, giving FIR filters with 15 coefficients.

4.1. TRANSIENT EXCITATION

Two transient, burst-random excitations are assumed to act on the beam. The first, applied at $x = -10\lambda_n$ is non-zero only for time steps such that $1000 \leqslant t_n \leqslant 1250$, while the second is applied at $x = 8\lambda_n$ and non-zero only for time steps such that $1350 \leqslant t_n \leqslant 1600$. The waves produced by these excitations propagate towards the origin where the response quantities are calculated. Both forces are random, Gaussian noise with unity variance which is band-pass filtered using a 21-term Parks–McClellan FIR filter designed using the

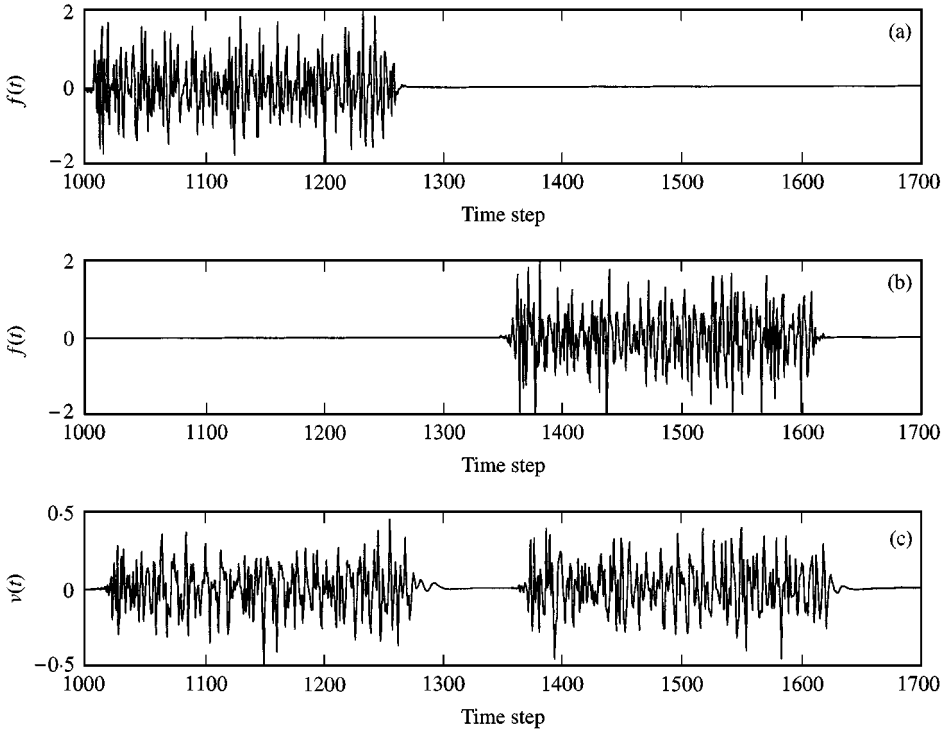

Figure 7. Time histories of (a) force at $x = -10\lambda_n$, (b) force at $x = 8\lambda_n$ and (c) velocity at $x = 0$

Matlab "*remez*" function. The filter has cut-off frequencies at $0{\cdot}15f_n$ and $0{\cdot}85f_n$ respectively.

Figure 7 shows the applied forces and the velocity at $x = 0$ as functions of time. There is a noticeable time delay before the waves excited by each force arrive at the response point, with the higher and lower frequency components arriving earlier and later respectively.

Figure 8 shows the actual shear force at $x = 0$ and that predicted using the wave decomposition and reconstruction technique. In the latter case, the time axis is shifted by $r = 7$ steps, this being the group delay introduced by the filters. For filters of the length used here the two are virtually identical, noticeable differences being primarily at the beginning and end of the bursts. Estimates of the bending moment at $x = 0$ are of comparable accuracy, while those of the velocity and slope are substantially more accurate. The standard deviations of the errors for this particular simulation are given in Table 1.

Once the beam displacement and slope and the internal forces have been estimated, they can be multiplied to yield estimates of the intensity. In Figure 9 the actual intensity at $x = 0$ and the wave decomposition estimate found from the sum of the shear and bending components, time-shifted by r steps once again are shown. The individual components of intensity are shown in Figure 10. The intensity is clearly positive or negative during those time periods during which waves arrive from the forces at $x < 0$ and $x > 0$ respectively. Again the agreement is excellent.

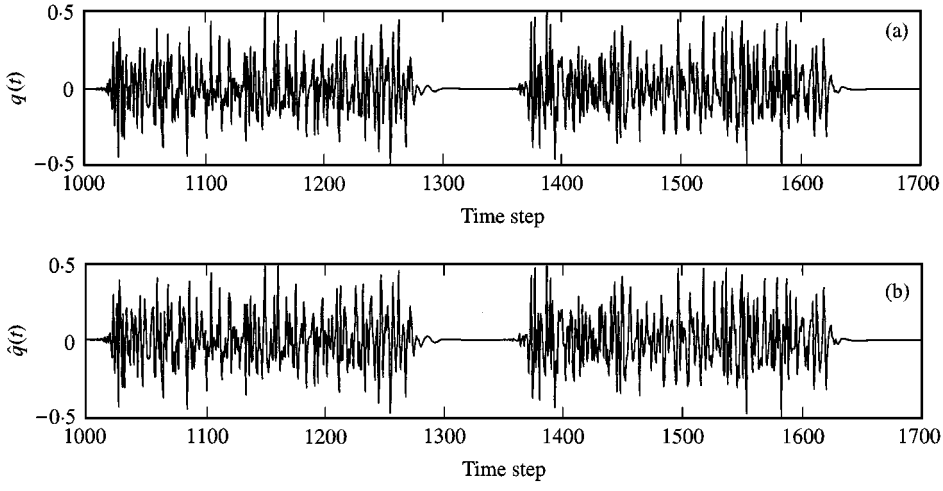

Figure 8. Time histories of (a) actual and (b) (time-shifted) estimated shear force at $x = 0$.

TABLE 1

Normalized standard deviation $\sigma_p = \sqrt{\overline{(\hat{p} - p)^2}} / \sqrt{\overline{p^2}}$ *of response variables* $\hat{p}$, *normalized with respect to actual variable* p, *for signal bursts in section* 4.1

Variable	σ_p (%)
v	0·172
$\dot{\theta}$	0·043
m	7·97
q	7·38
i	4·21

The individual components of intensity (Figure 10) are similar in magnitude to the total intensity and clearly fluctuate more rapidly with time.

Figure 9 also shows the finite difference expression of equation (4), whose time average equals that of the actual intensity. This illustrates one problem with this finite difference approximation: the intensity is estimated by finding the mean of a quantity which is both positive and negative, and whose amplitude is typically an order of magnitude greater than the actual intensity, thus making it prone to measurement errors, phase inaccuracies and so on.

The components of intensity associated with the positive- and negative-going waves individually can be found using the power wave filters of equation (27). The estimates of these directional components of intensity are shown in Figure 11. They can be clearly identified as being caused by the individual force bursts.

4.2. TIME AVERAGES: NOISE AND MIS-CALIBRATION

In this section only the random, band-limited force at $x = -10\lambda_n$ is applied. Now, however, it is random, stationary and continuous. The intensity is therefore

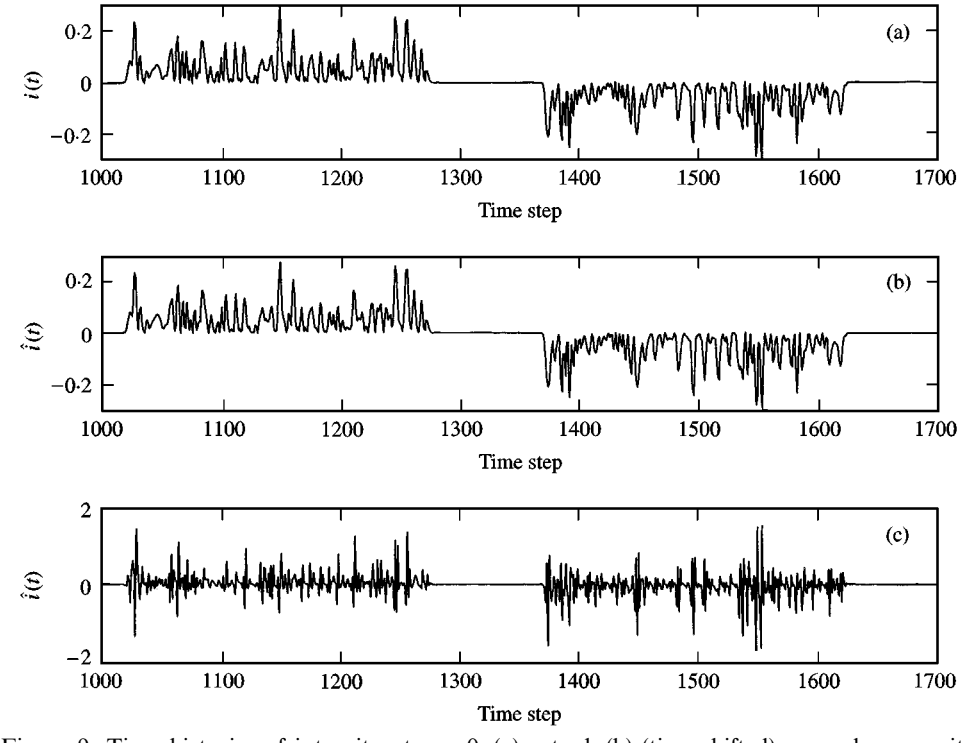

Figure 9. Time histories of intensity at $x = 0$: (a) actual; (b) (time-shifted) wave decomposition estimate; (c) finite difference approximation, equation (4).

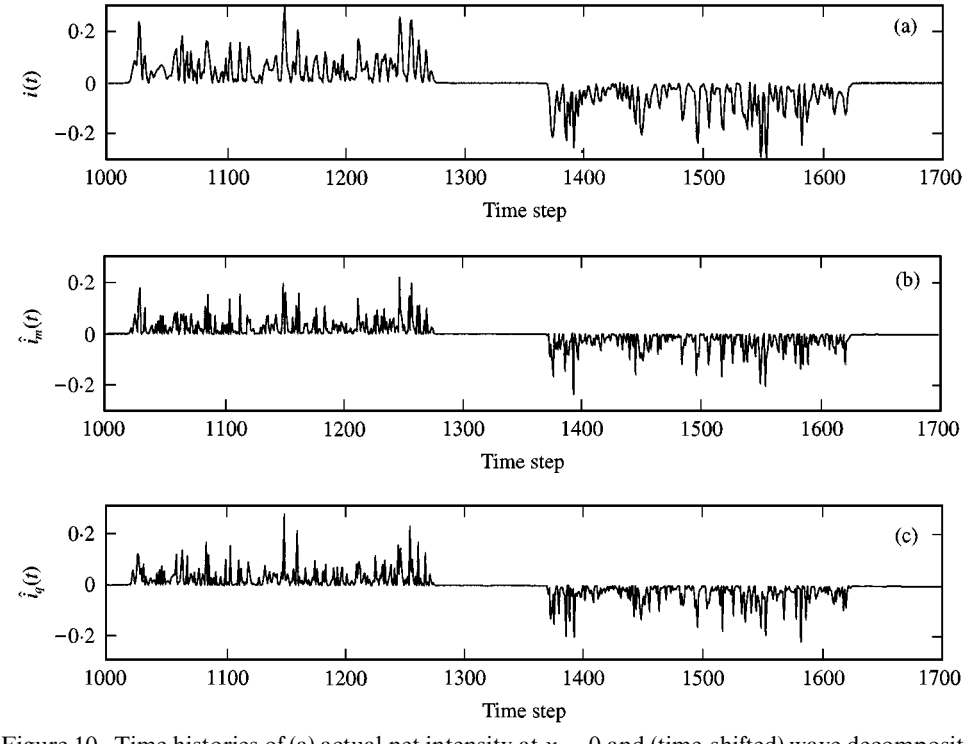

Figure 10. Time histories of (a) actual net intensity at $x = 0$ and (time-shifted) wave decomposition estimates of (b) moment and (c) shear component.

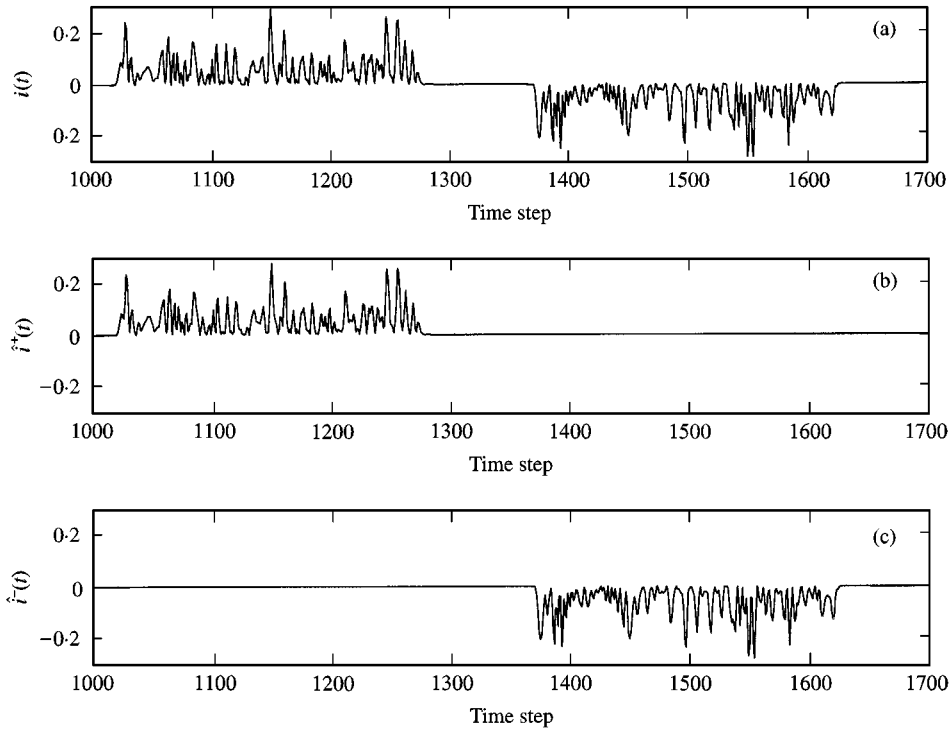

Figure 11. Time histories of (a) actual net intensity at $x = 0$ and (time-shifted) wave decomposition, power wave estimates of (b) positive-going component and (c) negative-going component.

also random. In this section time averages, found by taking moving averages over various numbers of points, will be investigated.

Typical time averages, taken over 101 and 301 points, are shown in Figure 12. Since the discrete time, wave decomposition estimates of intensity agree well with the true intensity so, too, do the time averages. Time averages of the finite difference approximation, equation (4), however, show substantially larger fluctuations together with a consistent bias error. This bias error is known to be due to the finite difference approximation (and is broadly dependent on $\sin k\Delta/k\Delta$) and increases as the sensor spacing increases.

Figure 13 illustrates the effects of measurement noise and miscalibration on the long-term time averages (taken over all 32 768 points). It is assumed that the measurement from the first sensor is accurate while the output of the second sensor is $\hat{v}_2(t) = (1 + \mu_m)\exp(\mathrm{i}\mu_p)(1 + \varepsilon_2(t))v_2(t)$. Here, μ_m and μ_P represent the effects of relative miscalibration on the magnitudes and phases of the sensors respectively, while $\varepsilon_2(t)$ is measurement noise, assumed to be Gaussian, of zero mean and of standard deviation σ_ε. Measurement noise does not substantially affect the long-term means, the main difference being that the variance about the mean becomes larger with increasing noise. Noise affects the finite difference average somewhat more. (The bias in the finite difference estimate is clear). The effects of magnitude miscalibration are also not profound and affect the estimates provided

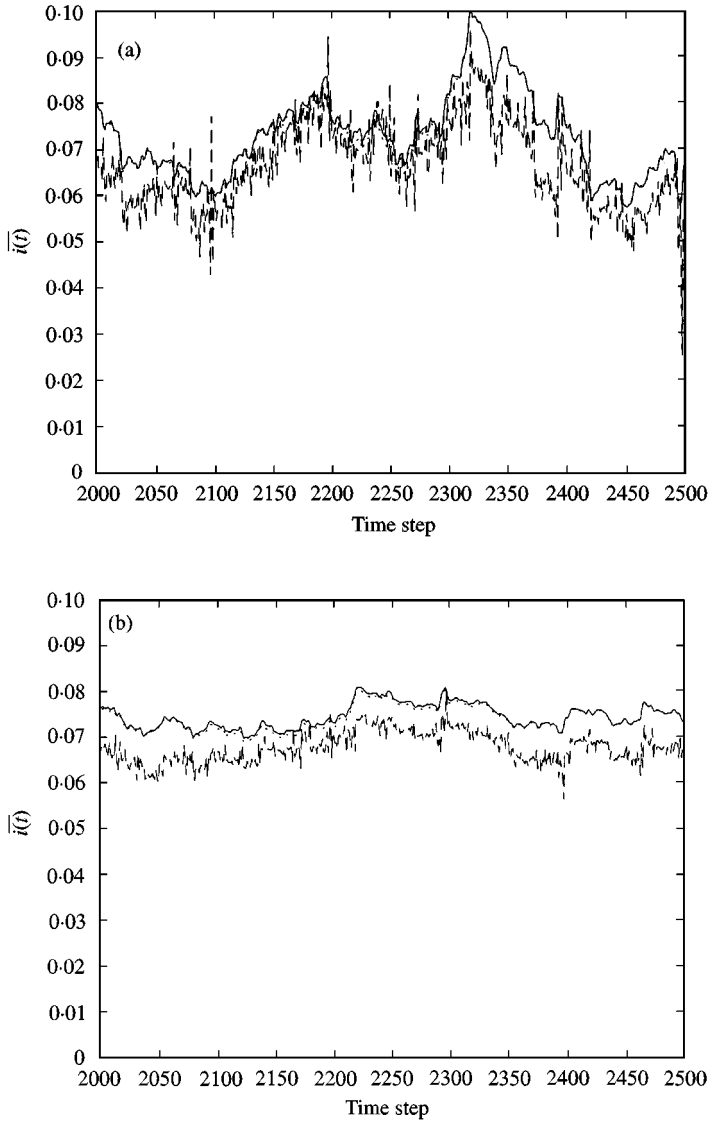

Figure 12. Time-average net intensity taken over (a) 101 and (b) 301 time steps: —, exact; ...., wave decomposition; - - - -, finite difference approximation.

by each method to a similar degree. The wave decomposition estimate, however, is very much less sensitive to phase miscalibration, where miscalibration of even a few degrees can produce extremely large errors in finite difference estimates. This sensitivity can be related to the fact that the allowable sensor spacing for the wave decomposition approach is so much larger: broadly, the spacing must be less than half a wavelength, whereas for the finite difference approach it must be small compared to a wavelength. Increasing the spacing reduces the sensitivity to phase miscalibration in the finite difference approach, but at the expense of increasing the bias.

5. IMPLEMENTATION AND EXPERIMENTAL MEASUREMENTS

5.1. EXPERIMENTAL SET-UP

Experimental measurements were performed on a steel beam to demonstrate the applicability of the technique described above. The beam had nominal dimensions of $6000 \times 50 \times 6$ mm and was suspended by piano wire at 1500 mm intervals along its length. The ends of the beam were embedded in sand to approximate anechoic terminations. The beam was excited near its centre by a non-contacting coil-and-magnet exciter, the applied force being measured with a Bruel and Kjaer

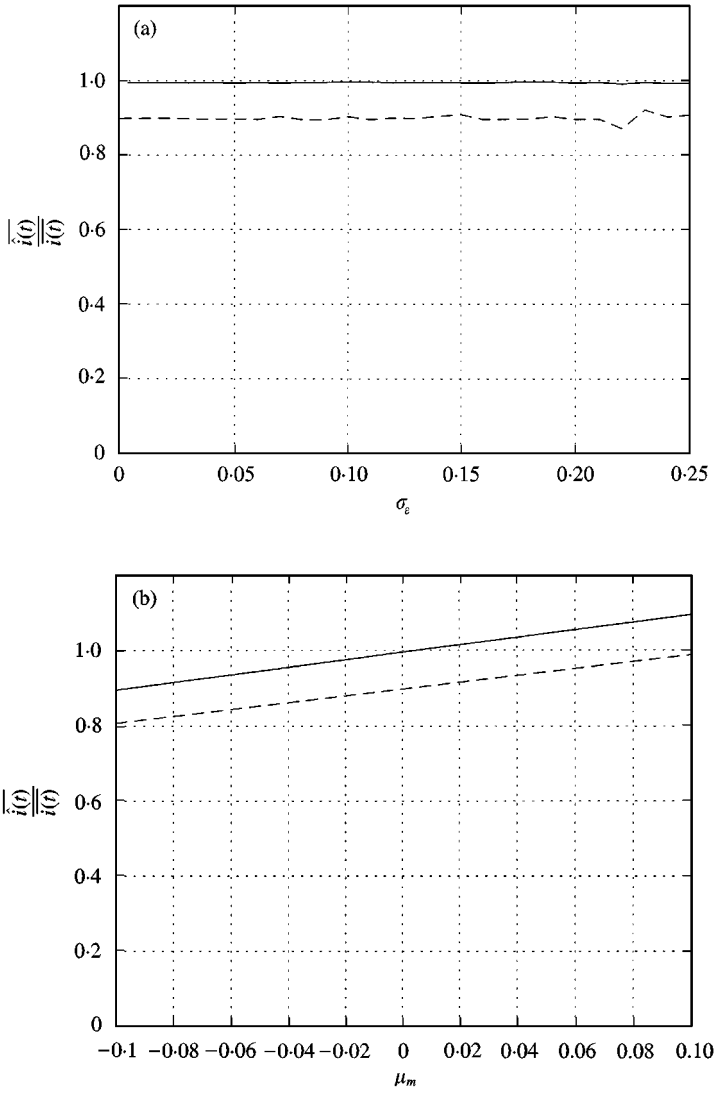

Figure 13. Effects on long-term time average of (a) noise on sensor 2, (b) magnitude miscalibration of sensor 2 and (c) phase miscalibration of sensor 2: —, wave decomposition; - - - - finite difference approximation.

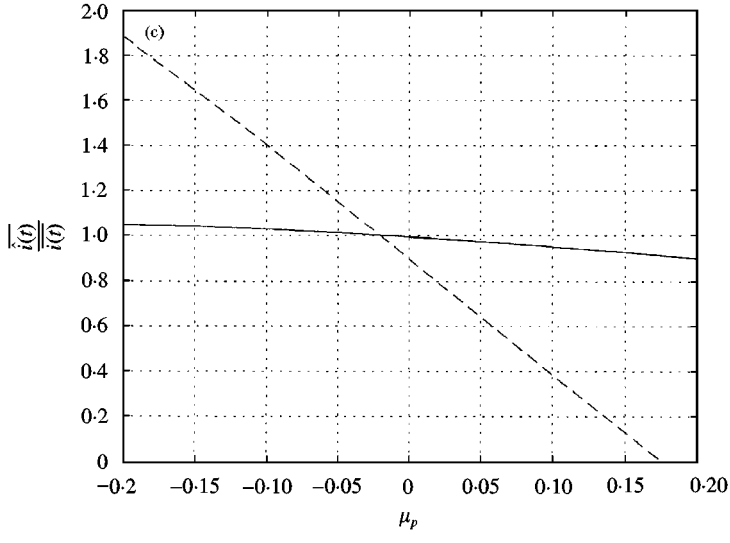

Figure 13. Continued.

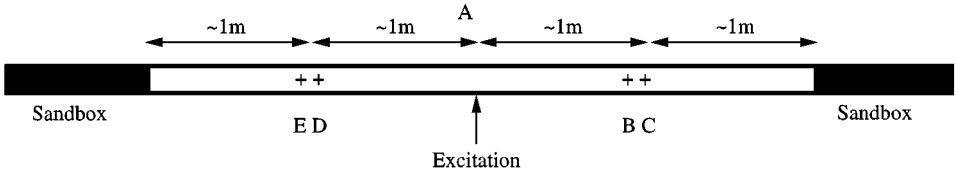

Figure 14. Schematic of experimental apparatus—locations of measurement points.

type 8200 force transducer. This experimental apparatus has been used extensively in vibrational energy flow measurements [4], and its behaviour is well documented.

The response of the beam was measured at the required points using an array of five PCB 353B65 accelerometers, in conjunction with a Hewlett–Packard HP3566A 8 Channel Dynamic Signal Analyser. All measurements were stored as time records, with subsequent processing performed using MATLAB software. The results therefore simulate the behaviour of a digital real-time (or real time plus delay) vibrational energy flow measurement system, since they are not subject to processing speed limitations. In practice, the required processing speed will be dependent on the sampling rate, the desired response quantities and on the number of terms in the digital filters that are necessary to approximate the desired frequency responses to the required accuracy. This will depend on the frequency band of interest, the types of sensors used and their placement and the signal conditioning that is used prior to digitization. For example, integration or filtering (after anti-alias filtering) may be performed using either analogue or digital

techniques. If these operations are to be performed digitally they may increase the length of the filters required, consequently increasing the processing time.

The input power to the beam was calculated from the measurements of input force and (digitally integrated) driving point acceleration. The vibrational energy flow was calculated, using the techniques described in this paper, from two relatively widely spaced measurements of acceleration in each arm of the beam (at points B and C, D and E—see Figure 14). The time average of the energy flow was compared with the time-averaged input power to investigate the accuracy of the energy flow measurement on average.

5.2. DIGITIZATION, PRE-PROCESSING AND DIGITAL FILTER DESIGN

As discussed in section 3, four filters are required to estimate the instantaneous components of intensity in the far field of a beam under flexural vibration. In the case where velocities are the measured variables, the required frequency responses are given by equations (25). If, however, other variables are measured the filters are required to have different frequency responses. In these experimental measurements two cases are considered. In the first of these the measurements of acceleration are digitized directly, while in the second analogue integration is used to provide velocity measurements.

The frequency range of interest will determine the minimum rate at which the sensor outputs must be sampled. Analogue low-pass filters must be used prior to digitization to avoid aliasing. If real-time processing is required it will usually be advantageous to minimize the sampling rate, thereby maximizing the processing time available between samples. In addition, bandpass filtering may also be required, as noted in section 3.4. The optimum spacing of the sensors is related to the frequency range of interest. As the sensor spacing becomes very small relative to a wavelength, or approaches a half-wavelength, the calculation of some of the required variables (linear and rotational velocity, bending moment and shear force) become extremely sensitive to noise and other measurement errors. Poor conditioning at high frequencies can be avoided by using a sensor spacing that gives acceptable conditioning up to the cut-off frequency of the anti-aliasing filters, or lower if additional filtering, either digital or analogue, is applied. There will also be a low-frequency limit below which the conditioning becomes unacceptable. The presence of noise at these low frequencies can contribute significantly to errors in the measurement, and thus their attenuation by high-pass filtering may be advisable. This filtering may be performed using either analogue or digital techniques. However, provided that the inclusion of bandpass filtering in the digital stage does not cause an unacceptable increase in the processing requirements, digital filtering can provide significant advantages over its analogue equivalent, including the ability to tailor the filter characteristics for individual applications.

In the experiments described below the measured data was bandpass filtered digitally to attenuate components below $0{\cdot}15f_n$ and above $0{\cdot}85f_n$. This was achieved using the same bandpass filters used for the numerical simulations. The

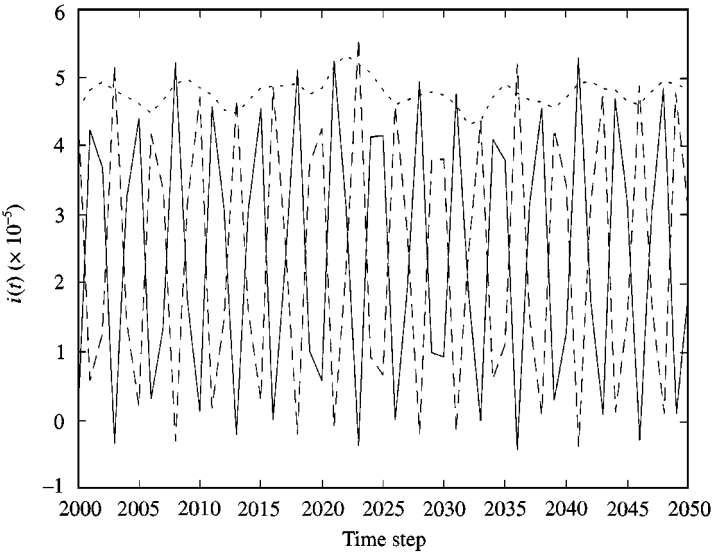

Figure 15. Time histories of wave decomposition intensity estimates, time harmonic excitation at 310 Hz, acceleration measurements: ...., total intensity; —, shear component; ----, moment component.

filtering reduces signal levels in the frequency ranges where the measurement system is poorly conditioned.

The same FIR filters as those used in the numerical simulations above were used to process the measured velocity signals (i.e., filters with $r = 7$), except that the weight function was set to zero outside the pass band of interest. When acceleration signals are used, filters of this length give somewhat reduced accuracy, due to the emphasis acceleration signals place on the high-frequency components.

5.3. EXPERIMENTAL RESULTS

A sampling rate of 2048 Hz was used for each of the two measurement schemes (acceleration inputs and velocity inputs), with a sensor spacing of 90 mm, corresponding to 0·76 rad at 100 Hz and 2·27 rad at 900 Hz. In each case, the beam was subjected first to sinusoidal excitation at selected frequencies, and then to random excitation in the frequency band 0–800 Hz.

Figures 15 and 16 show examples of the instantaneous estimates of the shear and moment components of intensity and the total intensity in the right arm of the beam under sinusoidal excitation at 310 Hz, as derived from acceleration and velocity inputs respectively. In each case, it is apparent that the shear and moment components are of comparable magnitude, opposite phase, and vary between zero and a maximum value, as would be expected. Figures 17 and 18 show the instantaneous intensity under random excitation for the two measurement schemes. The instantaneous intensity is occasionally negative due to the fact that the end of the beam is not perfectly anechoic. For the case of time harmonic

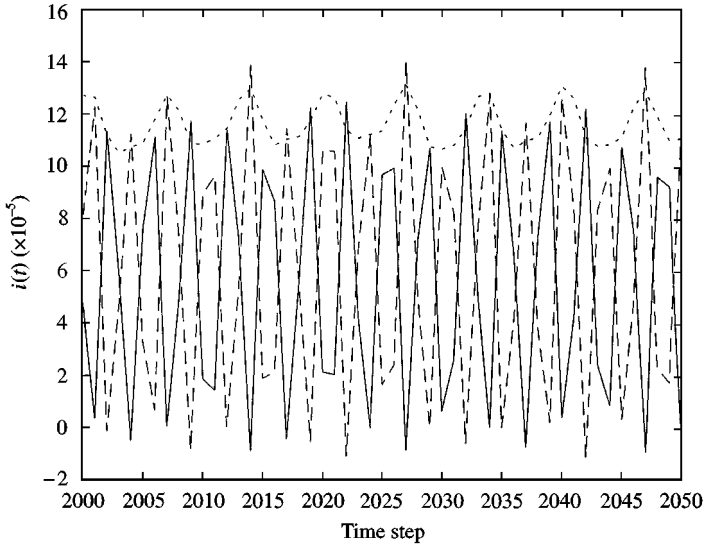

Figure 16. Time histories of wave decomposition intensity estimates, time harmonic excitation at 310 Hz, velocity measurements: ...., total intensity; —, shear component; - - - -, moment component.

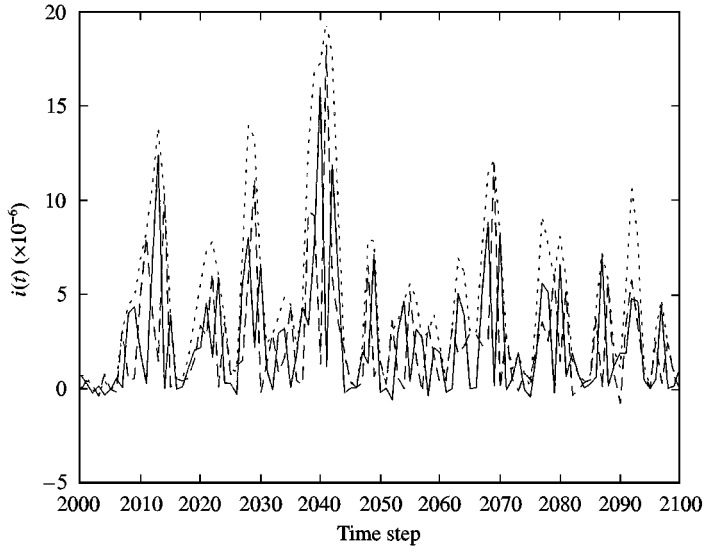

Figure 17. Time histories of wave decomposition intensity estimates, random excitation, acceleration measurements: ...., total intensity; —, shear component; - - - -, moment component.

excitation, the total instantaneous intensity shows some small fluctuations due to filtering approximations.

It should be noted that the individual components of intensity vary at twice the excitation frequency, and thus, for excitation frequencies greater than half the Nyquist frequency, some visual aliasing will occur. Thus, while there is sufficient information to define the components unambiguously, care should be exercised in the interpretation of "as plotted" data.

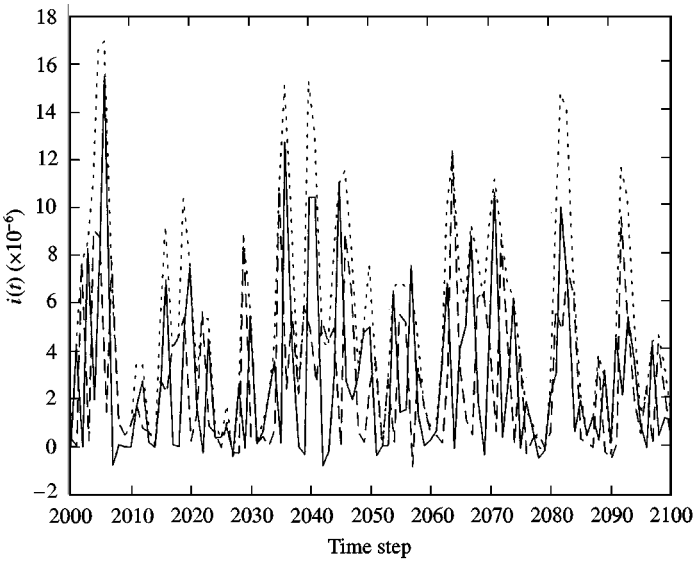

Figure 18. Time histories of wave decomposition intensity estimates, random excitation, velocity measurements: ...., total intensity; —, shear component; ----, moment component.

In all cases the agreement between time-averaged input power and time-averaged total energy flow (i.e., the time-average of the sum of the individual components of instantaneous intensity in each arm of the beam) was within 10%.

6. CONCLUDING REMARKS

In this paper a technique was described by which various response quantities may be estimated. The approach is based on wave decomposition and reconstruction, design being carried out in the frequency domain and implemented in the time domain using digital filters. The case of bending vibrations in beams was considered, although the technique is applicable to any wave-bearing structure. Emphasis was placed on the estimation of intensity, its shear and moment components and the components which propagate in different directions. Numerical simulations and experimental demonstration were described.

The particular advantages of the method include the fact that it is systematic, allowing sensor systems of arbitrary types, and that the wave decomposition approach enables sensors to be optimally spaced, reducing sensitivity to noise and miscalibration.

ACKNOWLEDGMENTS

The authors gratefully acknowledge the financial assistance provided by the New Zealand Foundation for Research, Science and Technology.

REFERENCES

1. G. Pavic 1976 *Journal of Sound and Vibration* **49**, 221–230. Measurement of structure borne wave intensity, Part 1: formulation of the methods.
2. W. Redman-White 1983 The measurement of structural wave intensity. Ph.D. Thesis, University of Southampton.
3. J. W. Verheij 1980 *Journal of Sound and Vibration* **70**, 133–138. Cross spectral density methods for measuring structure borne power flow on beams and pipes.
4. C. R. Halkyard and B. R. Mace 1995 *Journal of Sound and Vibration* **185**, 279–298. Structural intensity in beams—waves, transducers and the conditioning problem.
5. G. P. Gibbs, C. R. Fuller and R. J. Silcox 1993 *Proceedings of the 2nd Conference on Recent Advances in Active Control of Sound and Vibration*, Blacksburg, VA, 909–925. Active control of flexural and extensional power flow in beams using real time wave vector sensors.
6. G. P. Gibbs and C. R. Fuller 1994 *Proceedings of the 4th International Conference on Structural Intensity*, Senlis, France, 127–136. A "real time" wave vector filter for one dimensional structural media.
7. R. Kuc 1988. *Introduction to Digital Signal Processing*. New York: McGraw-Hill.
8. J. Doyle 1989. *Wave Propagation in Structure, an FFT-based Spectral Analysis Methodology*. New York: Springer-Verlag.

APPENDIX: NOMENCLATURE

The lower-case symbol (e.g., $p(t)$) is used to represent a variable in the time domain, while the upper case, $P(\omega)$, represents the same variable in the frequency domain.

a	acceleration
EI	bending stiffness
f	frequency, force
f_n	Nyquist frequency
f_s	sampling frequency
h	filter impulse response, FIR filter coefficient
H	filter frequency response
i	intensity
k	wavenumber
m	bending moment
n	time step
p	arbitrary variable, distributed load
q	shear force
r	filter delay
s	sensor output
t	time
v	velocity
w	displacement
x	position along beam
Δ	sensor separation
θ	beam rotation
λ	wavelength
ρ	mass per unit length
σ	filter weight function
τ	sampling time, $1/f_s$

ϕ wave amplitude
ω frequency

Subscripts

j sensor number
k filter coefficient number
m time step number
n Nyquist frequency
N near field
s sampling frequency